Chinese Chemical Letters 36 (2025) 109904

Contents lists available at ScienceDirect

Chinese Chemical Letters

journal homepage: www.elsevier.com/locate/cclet

Viscosity-responsive signal amplification dual-modal probe triggered by cysteine/homocysteine for monitoring diabetic liver damages and repair processes

Sixin Ai, Wenxiu Li, Huayong Zhu, Yang Wan, Weiying Lin*

Institute of Optical Materials and Chemical Biology, Guangxi Key Laboratory of Electrochemical Energy Materials, School of Chemistry and Chemical Engineering, Guangxi University, Nanning 530004, China

ARTICLE INFO

Article history:
Received 8 February 2024
Revised 12 April 2024
Accepted 16 April 2024
Available online 17 April 2024

Keywords:
Cysteine/homocysteine
Viscosity responsive
Near-infrared fluorescence
Photoacoustic imaging
Fluorescence imaging

ABSTRACT

Diabetic liver injury is a widespread complication of diabetes and carries a high risk to liver function. Therefore, early diagnosis of diabetic liver injury is of great significance for providing quality of life for diabetic patients. Most of the activated dual-modal probes are usually activated by single factor stimulation, which greatly reduces the diagnostic accuracy of liver injury. Here, a novel cysteine (Cys)/homocysteine (Hcy) and viscosity-enhanced dual-modal probe **DAL** was developed for the first time to monitor diabetic liver injury and its repair process. In the presence of Cys/Hcy, the near-infrared fluorescence (NIRF) and photoacoustic (PA) signals of the probe **DAL** were activated, with further signal enhancement in high viscosity environments. This Cys/Hcy and viscosity cascade probe exhibits heightened sensitivity and enhanced anti-interference capabilities, contributing to the advancement of liver injury diagnosis accuracy. In addition, the probe **DAL** shows exceptional mitochondrial targeting ability, enabling sensitive monitoring of Cys/Hcy and viscosity alterations within mitochondria. Based on NIRF/PA dual-modal imaging technology, the probe was successfully used for the first time in a mouse diabetic liver injury model to evaluate the extent of liver damage and the repair process by tracking the levels of Cys/Hcy and viscosity. Therefore, the two-factor activated dual-modal probe developed in this study provides a powerful instrument for accurate diagnosis and efficacy evaluation of complications related to diabetes.

Diabetes is a common metabolic disease, which is mainly characterized by insufficient insulin secretion or decreased insulin action, resulting in high blood sugar levels [1–3]. At present, the rifeness of diabetes is increasing worldwide, with about 422 million people affected by diabetes, and it has become a global health problem [4–6]. In addition, long-term diabetes can lead to various complications, including cardiovascular diseases, kidney failure, blindness, neuropathy, and liver damage [7,8]. Among these, the liver damage caused by diabetes is one of the main issues faced by individuals with diabetes [9,10]. Diabetic liver injury may lead to the development of liver cancer, liver tissue inflammation, fibrosis, and non-alcoholic fatty liver disease, which poses a great threat to human health [11,12]. Therefore, early and accurate diagnosis of liver damage caused by diabetes is crucial for the early warning and treatment of liver disease. To date, diagnostic techniques for diabetic liver injury have mainly focused on staining of tissue sections and the use of different assay kits to determine relevant biomarkers [13–16]. However, these traditional detection methods have some limitations and cannot reflect the pathological development process of diabetes-related liver damage in real-time and non-invasively [17]. Therefore, there is an urgent need to develop a non-invasive and multimodal method to accurately diagnose the degree of liver damage and the repair process caused by diabetes.

In recent years, near-infrared fluorescence (NIRF) imaging technology has gained widespread recognition for *in vivo* imaging owing to its high sensitivity, non-invasive capabilities, and high-resolution imaging [18–22]. However, NIRF imaging is still constrained by limited penetration depth and low spatial resolution [23–26]. Compared to fluorescence imaging, photoacoustic (PA) imaging combines optical and ultrasonic imaging with deeper imaging depth, can provide three-dimensional (3D) images with very high imaging depth, and depicts deep tissue structure with microscopic dimensional resolution but has the shortcomings of low sensitivity [27–30]. Therefore, the complementary strategy of integrating NIRF and PA imaging can overcome the inherent limitations of single-mode imaging and improve the sensitivity and

* Corresponding author.
E-mail address: weiyinglin2013@163.com (W. Lin).

https://doi.org/10.1016/j.cclet.2024.109904
1001-8417/

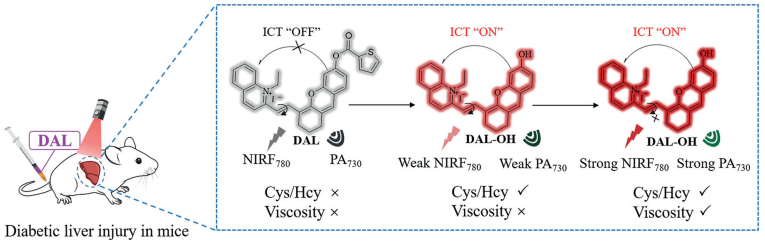

Scheme 1. Rational designs of the NIRF/PA probe **DAL** reporting Cys/Hcy and viscosity.

spatial resolution of deep tissue imaging *in vivo*. Currently, based on the merits of NIRF/PA dual-modal imaging, some dual-modal probes activated by a single disease biomarker have been developed for non-invasive imaging of liver injury [31]. However, probes based on single-factor activation are often susceptible to interference from the biological microenvironment and may sometimes face drawbacks such as weak signals and low sensitivity, which are not conducive to accurate diagnosis of complex diseases [32–34]. Cysteine/homocysteine (Cys/Hcy) is a common amino acid in living organisms and plays a significant part in regulating redox homeostasis during physiological processes [35,36]. Studies have found that the elevated levels of Cys/Hcy are closely associated with diabetic liver injury [37–40]. It is worth noting that in the pathogenesis of diabetic liver injury, superabundant accumulation of hepatocyte lipids is accompanied by changes in the intracellular microenvironment [41,42]. Increased viscosity in cells is an important feature of diabetic liver injury [43]. Therefore, the development of a Cys/Hcy triggered viscosity response signal amplification dual-mode probe is of great importance for the diagnosis and cure of diabetic liver injury. Until now, no probe capable of detecting both Cys/Hcy and viscosity has been reported.

In this work, we have developed a Cys/Hcy and viscosity cascaded NIRF and PA dual-mode probe **DAL** for precise diagnosis of diabetes liver damage and repair processes, for the first time. The probe **DAL** consists of a thiophene-2-carbonyl group (Cys/Hcy recognition unit) and a cyanine-like dye (**DAL-OH**, viscosity-sensitive dye platform). The NIRF/PA signals of probe **DAL** would be in the "off" state because of the restrain of the ICT effect by the thiophene-2-carbonyl chloride group. The **DAL** can selectively recognize Cys/Hcy at the spot of liver injury, thereby releasing the NIRF and PA signal of the dye **DAL-OH**. Simultaneously, the NIRF and PA signals of **DAL-OH** are further amplified in the high-viscosity environment of diabetes liver injury. Based on the strategy of Cys/Hcy and viscosity cascade reaction, this probe **DAL** will provide a promising tool for accurate diagnosis and therapeutic evaluation of diabetes liver injury. The synthesis routes and characterization of **DAL-OH** and **DAL** are described in Scheme 1 and Figs. S1–S8 (Supporting information).

First, we conducted a succession of *in vitro* experiments to further evaluate the photophysical properties of **DAL**. Its response to Cys/Hcy was evaluated in PBS (pH 8.0, 50% PBS/DMSO). After the increase of Cys/Hcy, the main absorption of **DAL** weakened at 554 nm, while new absorption peaks gradually appeared at 730 nm, indicating the formation of **DAL-OH** (Fig. 1A). Then, high-resolution mass spectrometry was used to attest the reaction mechanism. After the reaction of the probe **DAL** with excessive Cys/Hcy, a new mass peak was observed at 382.1810, which was attributed to the [**DAL-OH**] species (Fig. S9 in Supporting information). The results suggest that the probe **DAL** can respond to Cys/Hcy, leading to the release of **DAL-OH**. Furthermore, the absorption response of probe **DAL** to different concentrations of Cys/Hcy was studied. After adding diverse concentrations of Cys/Hcy in **DAL** solution (10 μmol/L), the absorption intensity increased at 730 nm and reached the highest at 200 μmol/L (Fig. S10 in Supporting information). Meanwhile, the Cys/Hcy concentration of **DAL** within the range of 0–80 μmol/L has a great linear relationship, and **DAL** has low detection limits of 0.55 μmol/L for Cys and 0.67 μmol/L for Hcy, indicating that the probe **DAL** can be utilized to monitor and track the levels of Cys/Hcy (Fig. S11 in Supporting information). The time-dependent absorption spectra of probe **DAL** show that the probe could rapidly analyze Cys/Hcy within roughly 40 min (Fig. S12 in Supporting information). Moreover, the absorption intensity of the free **DAL** remains essentially unchanged within 1.5 h. These results suggest that **DAL** exhibits rapid responsiveness to Cys/Hcy and demonstrates potential for long-term *in vivo* imaging.

Next, we investigated the NIRF and PA response of the probe **DAL** to various concentrations of Cys/Hcy. As shown in Figs. 1B and D, the NIR fluorescence intensity at 780 nm ($NIRF_{780}$) gradually increased as the concentration of Cys/Hcy increases from 0 to 200 μmol/L. Compared to the initial state of **DAL**, the $NIRF_{780}$ intensity increased by 6.3 and 5.3 times, respectively, after the probe reacted with Cys/Hcy (Fig. S13 in Supporting information). Furthermore, a robust linear correlation was observed between the $NIRF_{780}$ intensity and the concentration of Cys/Hcy (0–140 μmol/L), with a detection limit of 0.83 μmol/L for Cys and 0.72 μmol/L for Hcy (Figs. 1C and E). In addition, after incubation with different concentrations of Cys/Hcy (0–200 μmol/L), the photoacoustic intensity at 730 nm (PA_{730}) gradually increased (Figs. 1F and H). Compared to the initial state of **DAL**, the PA_{730} intensity increased by 12.3 and 10.5 times, respectively, after the probe reacted with Cys/Hcy (Fig. S14 in Supporting information). The detection limits were calculated to be approximately 0.45 μmol/L for Cys and 0.58 μmol/L for Hcy (Figs. 1G and I). These results confirm that the **DAL** probe has excellent photostability and can sensitively detect Cys/Hcy using bimodal NIRF and PA detection *in vitro*. To investigate the sensitivity of the dye **DAL-OH** to viscosity, we conducted fluorescence spectroscopy tests of **DAL-OH** under varying viscosity conditions. As shown in Fig. S15 (Supporting information), the fluorescence intensity of **DAL-OH** exhibits a good linear relationship with viscosity from 2.4 cp to 122.5 cp, indicating that **DAL-OH** exhibits a good response to viscosity *in vitro*. Then, the ultraviolet–visible (UV–vis) spectra of the **DAL** in the presence of Cys/Hcy were measured under high viscosity and low viscosity environments, respectively. Compared to low viscosity, the Abs_{730} intensity of **DAL** after responding to Cys and Hcy increases by 2.2 and 2.1 times under high viscosity conditions (Fig. 2A), indicating that Abs_{730} signal of probe in response to Cys/Hcy was further amplified at high viscosity. Subsequently, we studied the emission spectra of **DAL** in the presence to Cys/Hcy under different viscosity conditions. As shown in Figs. 2B–D, under low viscosity, the $NIRF_{780}$ intensity was weak. However, as viscosity gradually increasing, the $NIRF_{780}$ intensity significantly strengthens, resulting in a respective 2.5-fold and 2.7-fold increase of Cys and Hcy. These results indicate that the probe **DAL** can undergo a cascade response with Cys/Hcy and viscosity. In addition, the kinetic experiments between probe **DAL** and Cys/Hcy were studied in a DMSO system containing 50% glycerol. The kinetic experimental results indicate that as the reaction time between the probe **DAL** and Cys/Hcy increases, the $NIRF_{780}$

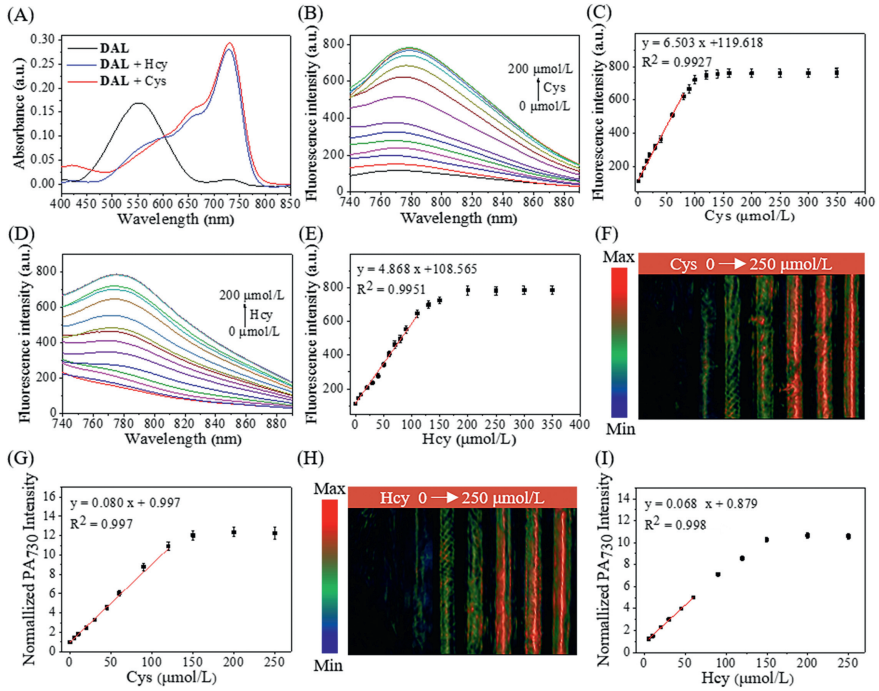

Fig. 1. *In vitro* photophysical properties of **DAL**. (A) UV–vis absorption spectra of the probe system (**DAL**, 10 μmol/L each) before and after adding Cys (200 μmol/L) and Hcy (200 μmol/L), respectively. (B) The fluorescence spectra of the **DAL** probe system (10 μmol/L each) were measured after incubation with different concentrations of Cys (0–200 μmol/L). λ_{ex} = 720 nm. (C) The plot of $NIRF_{780}$ intensity at Cys concentration of 0–200 μmol/L. (D) Fluorescence spectra of the probe **DAL** (10 μmol/L each) system after incubation with various concentrations of Hcy (0–200 μmol/L). λ_{ex} = 720 nm. (E) The plot of $NIRF_{780}$ intensity at Hcy concentration of 0–200 μmol/L. (F) Corresponding color PA_{730} images of the probe system reacting with various concentrations of Cys (0–200 μmol/L). (G) Relative PA_{730} intensities for the probe solution (**DAL**, 10 μmol/L each) as a function of the Cys concentration. λ_{ex} = 730 nm. (H) Corresponding color PA_{730} images of the probe system reacting with various concentrations of Hcy (0–200 μmol/L). (I) Relative PA_{730} intensities for the probe solution (**DAL**, 10 μmol/L each) as a function of the Hcy concentration. λ_{ex} = 730 nm. Data are presented as mean ± standard deviation (SD) (n = 3).

intensity signal gradually enhances and reaches a plateau within 40 min, demonstrating that **DAL** can rapidly identify Cys/Hcy (Fig. S16 in Supporting information). These findings demonstrate that the probe **DAL** has the potential for stable monitoring of Cys/Hcy and viscosity.

Finally, we investigated the selectivity of probe **DAL** by examining its response to different biological analytes in DMSO systems containing 50% glycerol. As shown in Fig. 2E and Fig. S17 (Supporting information), no other analytes except Cys/Hcy induced the reaction of **DAL**. This indicates that the probe can selectively identify Cys/Hcy. Next, we investigated the viscosity response of the dye **DAL-OH** in the presence of different analytes to investigate the anti-interference ability of **DAL-OH**. As shown in Fig. S18 (Supporting information), **DAL-OH** is not affected by other interfering analytes and exhibits good viscosity response at different viscosities, demonstrating its excellent anti-interference capability. We also investigated the cascade response of the probe to Cys/Hcy and viscosity under different pH conditions. As shown in Fig. 2F, the absorption signal of probe **DAL** almost remained unchanged at pH 3.0–10, demonstrating the good stability of the probe in different pH environments. Upon the addition of Cys/Hcy, the probe **DAL** exhibited a remarkable enhancement in the NIR signal at 730 nm within the pH range of 7.0–10.0. This indicates that **DAL** is capable of detecting Cys/Hcy under a broad range of physiological pH conditions. In addition, the lipophilicity of a compound is closely related to its diffusion and permeation into cell membranes. Therefore, we conducted a study on the lipophilicity (log$P$) of **DAL**. It is gratifying to find that **DAL** exhibits favorable characteristics in terms of lipophilicity (log$P$ = 2.55), falling within the optimal range (optimal log$P$ value between 2 and 4). This indicates that the probe **DAL** has the potential for a good balance between cell membrane permeability and intracellular stability.

Encouraged by the outstanding representation of the probe **DAL** *in vitro*, we investigated the fluorescence imaging of Cys/Hcy and viscosity in normal human hepatocyte cells (HL-7702 cell lines) using the probe **DAL**. Before the imaging in living cells, we assessed the dose-dependent toxicity of **DAL** on HL-7702 cell lines using standard MTT assays. As shown in Fig. S19 (Supporting information), the viability of these cell lines was as high as 80% at a concentration of 40 μmol/L **DAL**, suggesting that the probe showed very low cytotoxicity and preeminent biocompatibility. Due to the presence of a cationic quinoline unit in the probe **DAL**, it is expected that the probe will target mitochondria through electrostatic attraction interactions. Therefore, we conducted fluorescence co-localization experiments using a commercial organelle tracker (Mito Tracker green) to identify the mitochondrial targeting ability of the probe **DAL**. As shown in Fig. S20 (Supporting information), the red fluorescence observed from **DAL** overlaps well with the Mito Tracker green fluorescence signal, and the Pearson correlation coefficient (R) is as high as 0.85. The aforementioned outcomes demonstrate that the probe **DAL** accumulates within mitochondria and can precisely detect Cys/Hcy and viscosity in this organelle. These findings highlight the capacity of the probe **DAL** to serve as a potential tool in exploring the pathological link between Cys/Hcy and viscosity.

Inspired by the good biosafety of probe **DAL** *in vitro*, the NIRF/PA imaging of Cys/Hcy and viscosity in living cells by probe **DAL** was investigated. As shown in Fig. 3A, a weak fluorescence signal was observed after HL7702 cells were treated with probe **DAL** for 40 min. However, when the cells were pretreated with *N*-ethylmaleimide (NEM, a recognized thiol eliminator) and then treated with **DAL**, only negligible fluorescence was observed. These results evidenced that the probe is capable of imaging endogenous Cys/Hcy within the cells. Subsequently, cells were pretreated with

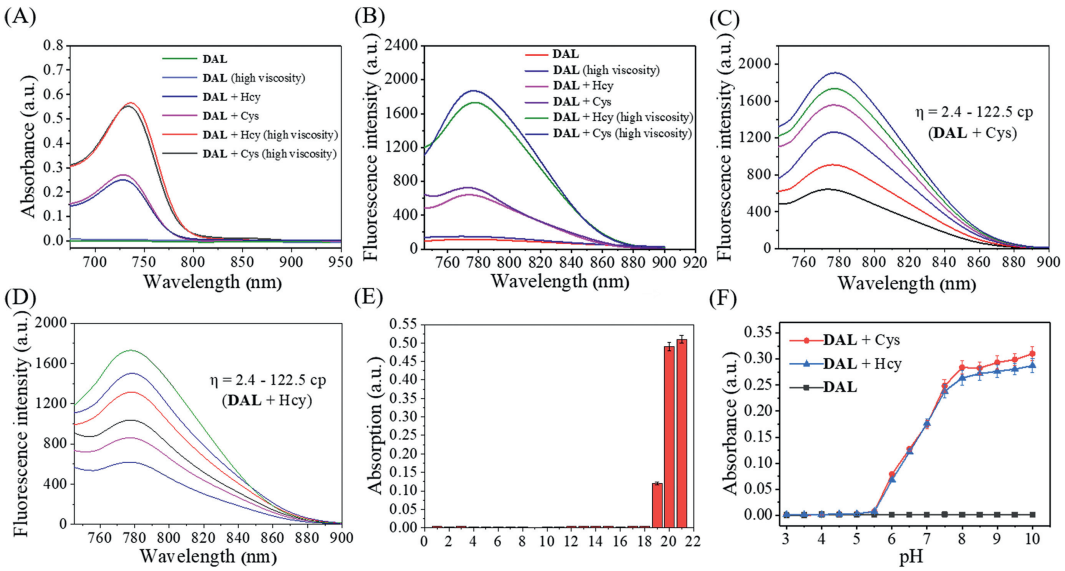

Fig. 2. The probe **DAL** viscosity response, suitability, and specificity. (A, B) In the presence or absence of Cys/Hcy in a DMSO system containing 50% glycerol and a DMSO system containing 50% PBS, the absorption (A) and fluorescence (B) spectra of the probe **DAL** (10 μmol/L) are shown. (C, D) Fluorescence response of the probe **DAL** after the addition of (C) Cys (200 μmol/L) and (D) Hcy (200 μmol/L) in an environment with different viscosities. (E) Absorption spectra of the probe DAL (10 μmol/L) were recorded in a DMSO/glycerol system (1/1, v/v) in the presence of various analytes (500 μmol/L each) including (1) H_2O_2, (2) Co^{2+}, (3) Cu^{2+}, (4) Hg^{+}, (5) HS^{-}, (6) Mg^{2+}, (7) Mn^{2+}, (8) SO_3^{2-}, (9) OAc^{-}, (10) $S_2O_3^{2-}$, (11) Ser, (12) Zn^{2+}, (13) His, (14) Aln, (15) Asp, (16) Br^{-}, (17) Ca^{2+}, (18) blank, (19) GSH, (20) Hcy (200 μmol/L) and (21) Cys (200 μmol/L) ($n = 3$). (F) The effect of absorption intensity of **DAL** (10 μmol/L) with Cys/Hcy (200 μmol/L) at different pH values ($n = 3$). Data are presented as mean ± SD.

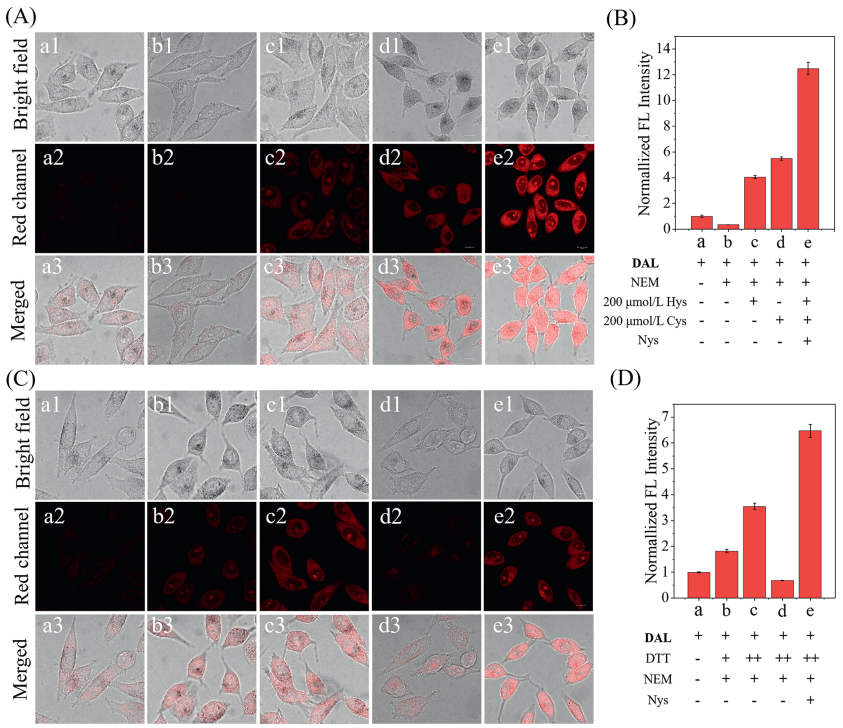

Fig. 3. Imaging of Cys/Hcy and viscosity in living cells. (A) Different treatments of cells in bright-field and fluorescence images: (a) cells treated with probe **DAL** (10 μmol/L) for 40 min; (b) cells pretreated with NEM (30 μL, 1 mmol/L) for 30 min, then treated with probe **DAL** (10 μmol/L) for 40 min; (c) cells preprocessed with NEM (30 μL, 1 mmol/L) for 30 min, then preprocessed with Hcy (200 μmol/L) and probe **DAL** (10 μmol/L) for 40 min; (d) cells preprocessed with NEM (30 μL, 1 mmol/L) for 30 min, then pretreated with Cys (200 μmol/L) and probe **DAL** (10 μmol/L) for 40 min; (e) cells preprocessed with NEM (30 μL, 1 mmol/L) for 30 min, then treated with Nys (20 μmol/L) and Cys/Hcy (200 μmol/L) for 30 min, and then treated with **DAL** probe (10 μmol/L) for 40 min. (B) Quantification of fluorescence intensity in (A) ($n = 3$). (C) Different treatments of cells in bright-field and fluorescence images: (a) cells treated with probe **DAL** (10 μmol/L) for 40 min; (b) cells preprocessed with NEM (30 μL, 1 mmol/L) for 30 min, then treated with DTT (0.1 mmol/L) for 30 min, and then treated with probe **DAL** (10 μmol/L) for 40 min; (c) cells preprocessed with NEM (30 μL, 1 mmol/L) for 30 min, then treated with DTT (0.2 mmol/L) for 30 min, and then treated with probe **DAL** (10 μmol/L) for 40 min; (d) cells preprocessed with DTT (0.2 mmol/L) for 30 min and treated with NEM (30 μL, 1 mmol/L) for 30 min, and then treated with probe **DAL** (10 μmol/L) for 40 min; (e) cells preprocessed with NEM (30 μL, 1 mmol/L) for 30 min, then treated with Nys (10 μmol/L) and DTT (0.2 mmol/L) for 30 min, and then treated with probe **DAL** (10 μmol/L) for 40 min. (D) Quantification of fluorescence intensity in (C) ($n = 3$). Red channel: $\lambda_{ex} = 660$ nm, $\lambda_{em} = 730$–790 nm. Scale bar: 10 μm. Data are presented as mean ± SD.

Cys/Hcy (200 μmol/L) for 30 min, followed by incubation with the **DAL** for 40 min. It was observed that the red NIRF signal was significantly enhanced (Fig. 3A), indicating that the probe **DAL** could image Cys/Hcy in living cells. Subsequently, we employed nystatin (Nys) to stimulate an elevation in intracellular viscosity to further explore the impact of viscosity on fluorescence intensity. Strikingly, cells treated with Nys + Cys/Hcy demonstrated a significant increase in red fluorescence upon incubation, with a 12.5-fold enhancement in fluorescence intensity compared to cells treated with the probe **DAL** alone (Fig. 3B). These results indicate that the fluorescence of probe **DAL** can be opened by exogenous Cys/Hcy and further amplified in high-viscosity cellular environment.

Then, we investigated the potential of probe **DAL** for NIRF/PA imaging of endogenous Cys/Hcy and viscosity in living cells. Nys as an ion carrier may disrupt mitochondrial ion homeostasis, leading to viscosity changes and impaired mitochondrial function. In cells, dithiothreitol (DTT) is a reagent that can induce an increase in Cys/Hcy concentration, thereby increasing endogenous Cys/Hcy levels [44]. As shown in Fig. 3C and Fig. S21 (Supporting information), after incubation with **DAL** for 40 min, HL-7702 cells showed no significant NIRF and PA signals. Nevertheless, when cells treated with different concentrations of DTT were incubated with probe **DAL** for 40 min, it was observed that NIRF and PA signals increased with increasing DTT concentration. In addition, after treating cells with DTT, the cells were incubated with NEM for 30 min to eliminate intracellular Cys/Hcy and a significant reduction in NIRF and PA signals was observed. Furthermore, it is worth noting that when cells were treated with Nys, enhanced NIRF and PA signals were observed, with a 6.5 times enhancement in NIRF signals and 4.3 times enhancement in PA signals compared to cells treated with probe **DAL** alone (Fig. 3D). These results are consistent with the phenomenon of extracellular experiments, further proving that the probe can be activated by endogenous Cys/Hcy produced by cells, achieving bimodal imaging of Cys/Hcy in cells, and the NIRF and PA signals of **DAL** can be amplified based on the increase of viscosity. This signal amplification capability enables the probe **DAL** to have higher sensitivity and prevents erroneous judgment results caused by a single response signal.

To investigate the potential of **DAL** for NIRF/PA dual-mode imaging of Cys/Hcy and viscosity *in vivo*, we conducted imaging studies *via* subcutaneous injection of **DAL** and exogenous Cys/Hcy into mice. All animal experiments were reviewed and approved by the Animal Care and Experiment Committee of Guangxi University (protocol number: Gxu-2022–173). After injecting **DAL** into the area of interest in the legs of mice (control group), a weak NIRF signal was observed, indicating the presence of intrinsic Cys/Hcy in the mouse. However, when mice were pretreated with NEM before **DAL** treatment, the NIRF and PA signals were significantly lower than in the control group, indicating that endogenous Cys/Hcy can activate the NIRF/PA signals of **DAL** (Figs. 4A–C). Then, with the addition of Cys/Hcy, the NIR FL/PA signals gradually increased. Subsequently, we injected Nys (50 μmol/L, 100 μL) to induce an increase in viscosity in the leg tissue, further exploring the impact of viscosity on fluorescence intensity. Experimental results revealed that following treatment with Nys, the NIRF/PA signal was further amplified (Fig. 4D). These results demonstrate that the probe **DAL** can perform cascading imaging of Cys/Hcy and viscosity *in vivo*.

The excellent bimodal imaging performance of the probe in live cells and mice inspired us to perform NIRF and PA imaging of anomalous viscosity and Cys/Hcy in a diabetic liver injury model. Firstly, we established the diabetic mouse model by intraperitoneal injection of streptozotocin (STZ), and random blood glucose levels greater than or equal to 16.8 indicated successful model establishment (Fig. S22 in Supporting information). Subsequently, NIRF imaging was performed on different groups of mice, including healthy mice without treatment (control group), diabetic mice (diabetic group), and diabetic mice treated with metformin (diabetic + Met-group). Both the control group and the Diabetic group received a tail vein injection of **DAL** (30 μmol/L, 100 μL) while the mice in the treatment group received oral administration of metformin for 7 days before **DAL** (30 μmol/L, 100 μL) injection. As illustrated in Figs. 5A and B, upon the administration of **DAL** (30 μmol/L, 100 μL) into the tail vein of mice, a faint fluorescent signal was detected in the liver region of the control group (healthy mice), which gradually intensified over time. Conversely, the fluorescent signal observed in the liver region of diabetic mice injected with **DAL** (30 μmol/L, 100 μL) was substantially stronger compared to that of the control group, reaching maximum intensity within 2.5 h, indicative of a notable increase in Cys/Hcy levels and viscosity in the liver site of diabetic mice. For diabetic mice treated with metformin, the fluorescent signal in the liver region was significantly reduced, indicating a downregulation of Cys/Hcy and viscosity expression in mice that received treatment. Subsequently, to further validate the ability of the **DAL** probe to visualize Cys/Hcy and viscosity levels in diabetic liver injury, we conducted *in vitro* fluorescence imaging of the vital organs of mice 2.5 h post-injection of **DAL**. As depicted in Fig. S23 (Supporting information), the fluorescence signal in the livers of diabetic mice exhibited noticeable intensity compared to the control group. Additionally, the fluorescence signals in the liver of the treated group were markedly weaker than that in the diabetic group. These results further confirm the potential of probe **DAL** for the detection and imaging of diabetic liver injury.

PA imaging can provide 3D images with very high imaging depth and depict deep tissues with microscopic resolution. Based on the dynamic changes in Cys/Hcy and viscosity, PA imaging is further used to assess diabetic liver injury in mice. 3D PA imaging of the abdomen of mice treated differently was performed at 2.5 h after injecting **DAL** (30 μmol/L, 100 μL). The results showed a significantly enhanced PA signal in the diabetic group compared to the control group, with a 3.90-fold increase in PA_{730} intensity in the liver region (Figs. 5C and D). Additionally, as expected, the liver PA signal in the treatment group mice was lower than that in the diabetic group, consistent with the results of near-infrared fluorescence imaging. These findings suggest the potential of **DAL** to detect diabetic liver injury by monitoring abnormal levels of Cys/Hcy and viscosity in the liver through *in situ* NIRF and PA imaging.

To confirm the liver injury in diabetic mice, we performed hematoxylin and eosin (H&E) staining of liver tissue sections from different groups for histological analysis. As depicted in Fig. S24 (Supporting information), the liver tissue sections from the control group mice exhibited a normal morphology. In contrast, the liver tissue sections from the diabetic group mice displayed hepatocyte vacuolation and hepatocyte hydropic degeneration. However, the liver tissue sections from the treatment group mice demonstrated significant improvement in morphology, resembling that of the control group more closely. This is consistent with the imaging results, further demonstrating the potential of the NIRF/PA dual-modal probe **DAL** in diagnosing diabetic liver injury and evaluating drug efficacy. Additionally, to assess the biocompatibility of the probe, we conducted a histological analysis of the major organs of the mice. As shown in Fig. S25 (Supporting information), no significant abnormalities or damage were found in visceral organs, including the heart, spleen, lungs, and kidneys, suggesting that **DAL** had negligible biological toxicity. These results further demonstrate that **DAL** has good biological safety and holds great potential in detecting liver damage caused by diabetes.

In summary, we constructed for the first time a bimodal probe (**DAL**) based on Cys/Hcy and viscosity cascade reaction for monitoring diabetic liver injury and repair process. Probe **DAL** showed significant NIRF/PA dual signal response to Cys/Hcy, and the NIRF/PA signal is further amplified in high viscosity environments. This cas-

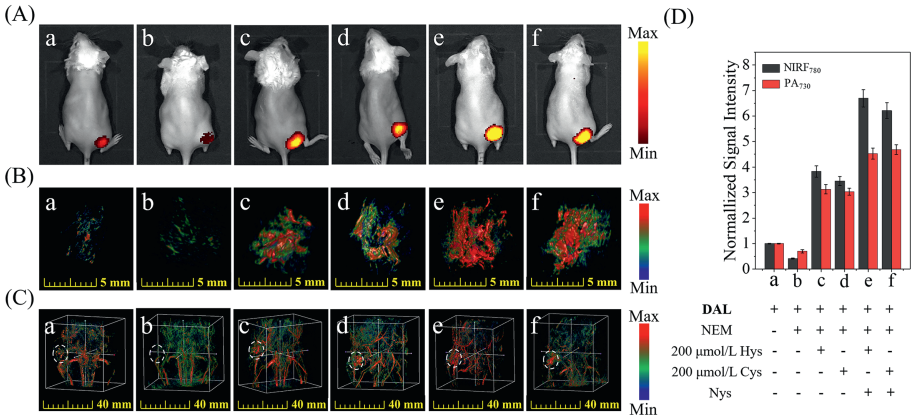

Fig. 4. Imaging of exogenous Cys/Hcy in live mice. (A) NIRF imaging of the mouse legs: (a) injection of the probe **DAL** (20 μmol/L, 100 μL) into the mouse legs; (b) the legs of the mouse preprocessed with NEM (30 μL, 1 mmol/L) for 3 h, followed by injection of the probe **DAL** (20 μmol/L, 100 μL); (c, d) the legs of the mouse were preprocessed with NEM (30 μL, 1 mmol/L) for 3 h, followed by injection of the probe **DAL** (20 μmol/L, 100 μL) and (c) Cys (400 μmol/L) or (d) Hcy (400 μmol/L); (e, f) the legs of the mouse were pretreated with Nys (50 μmol/L, 100 μL) for 24 h and then treated with NEM (30 μL, 1 mmol /L) for 3 h, followed by injection of the probe **DAL** (20 μmol/L, 100 μL) and (e) Cys (400 μmol/L) or (f) Hcy (400 μmol/L). E_x: 700 nm. (B) Exogenous cross-sectional PA imaging of the mouse legs is shown in (A) (scale bars: 5 mm). (C) 3D PA imaging of the mouse is shown in (B) (scale bars: 40 mm). (D) Normalized $NIRF_{780}$ and PA_{730} signal intensities from (A) and (B). E_x: 730 nm. Data are presented as mean ± SD ($n = 3$).

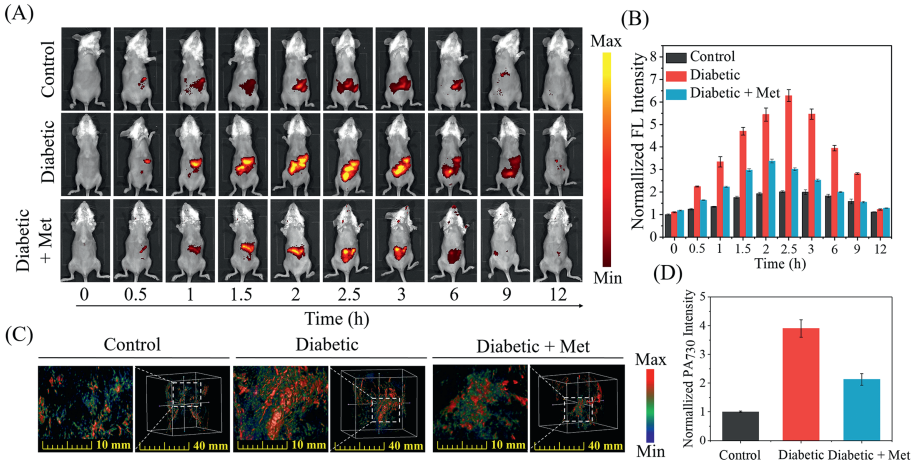

Fig. 5. NIRF and PA imaging in a mouse model of diabetic liver injury. (A) Different time points of NIRF images after intravenous injection of **DAL** (30 μmol/L, 100 μL) in the control group (healthy mice), diabetes group (diabetic mice), and diabetes + Met-group (diabetic mice treated with metformin). E_x: 700 nm. (B) $NIRF_{780}$ signal intensity values from (A) ($n = 3$). (C) *In vivo* PA_{730} imaging 2.5 h after intravenous injection of **DAL** (30 μmol/L, 100 μL) in the control group, diabetes group, and diabetes + Met-group. E_x: 730 nm; scale bars: 10 mm and 40 mm. (D) PA_{730} signal intensity values from (C) ($n = 3$). Data are presented as mean ± SD.

cade process of Cys/Hcy and viscosity gives the probe a stronger signal and excellent anti-interference capability. In addition, the **DAL** probe has demonstrated excellent mitochondrial targeting capabilities and can sensitively monitor the level changes of Cys/Hcy and viscosity in mitochondria. Based on the unique Cys/Hcy and viscosity cascade of the two-mode probe, we successfully used the probe for accurate diagnosis and efficacy evaluation of diabetic liver injury. We hope this work will provide new ideas and insights into the early diagnosis and pathogenesis of other diseases and their associated complications.

Declaration of competing interest

The authors declare that they have no known competing financial interests or personal relationships that could have appeared to influence the work reported in this paper.

CRediT authorship contribution statement

Sixin Ai: Writing – review & editing, Writing – original draft, Software, Methodology, Investigation, Formal analysis, Data curation. **Wenxiu Li:** Writing – review & editing, Writing – original draft, Methodology, Investigation, Formal analysis, Data curation, Conceptualization. **Huayong Zhu:** Software, Methodology, Investigation, Formal analysis. **Yang Wan:** Software, Methodology, Investigation, Formal analysis. **Weiying Lin:** Writing – review & editing, Writing – original draft, Validation, Supervision, Software, Resources, Project administration, Funding acquisition, Formal analysis, Data curation, Conceptualization.

Acknowledgments

This work was financially supported by the National Natural Science Foundation of China (Nos. 21877048, 22077048, and 22277014), Guangxi Natural Science Foundation (Nos. 2021GXNSFDA075003, AD21220061), and the Startup Fund of Guangxi University (No. A3040051003).

Supplementary materials

Supplementary material associated with this article can be found, in the online version, at doi:10.1016/j.cclet.2024.109904.

References

[1] Q. Chen, Y. Zhao, Y. Liu, Chin. Chem. Lett. 32 (2021) 3705–3717.
[2] A. Tan, X. Ma, Chin. Chem. Lett. 35 (2024) 109276.
[3] K. Ogurtsova, J.D.D.R. Fernandes, Y. Huang, et al., Diabetes Res. Clin. Pract. 128 (2017) 40–50.
[4] E.W. Gregg, N. Sattar, M.K. Ali, Lancet Diabetes Endocrinol. 4 (2016) 537–547.
[5] J.L. Harding, M.E. Pavkov, D.J. Magliano, et al., Diabetologia 62 (2019) 3–16.
[6] R.C.W. Ma, Diabetologia 61 (2018) 1491.
[7] J.M. Forbes, M.E. Cooper, Physiol. Rev. 93 (2013) 137–188.
[8] P. Manna, J. Das, J. Ghosh, et al., Free Radic. Biol. Med. 48 (2010) 1465–1484.
[9] K. Kubota, H. Watanabe, Y. Murata, et al., Nucl. Med. Biol. 38 (2011) 347–351.
[10] C. Buettner, R.C. Camacho, Endocrinol. Metab. Clin. North Am. 37 (2008) 825–840.
[11] R. Kakkar, S.V. Mantha, J. Radhi, et al., Clin. Sci. 94 (1998) 623–632.
[12] H.B. El-serag, T. Tran, J.E. Everhart, Gastroenterology 126 (2004) 460–468.
[13] I. Rasnik, S.A. McKinney, T. Ha, Nat. Meth. 3 (2006) 891–893.
[14] C. Wu, B. Bull, C. Szymanski, et al., ACS Nano 2 (2008) 2415–2423.
[15] H. Hama, H. Kurokawa, H. Kawano, et al., Nat. Neurosci. 14 (2011) 1481–1488.
[16] Y. Zhang, X. Wang, X. Bai, et al., Anal. Chem. 91 (2019) 8591–8594.
[17] E. Espinel, I. Agraz, M. Ibernon, et al., J. Clin. Med. 4 (2015) 998–1009.
[18] J. Zhang, L. Wang, A. Jäschke, et al., Angew. Chem. Int. Ed. 60 (2021) 21441–21448.
[19] H. Li, Y. Kim, H. Jung, et al., Chem. Soc. Rev. 51 (2022) 8957–9008.
[20] J. Wang, F. Huo, Y. Zhang, et al., Chin. Chem. Lett. 34 (2023) 107818.
[21] Y. Xu, C. Li, S. Lu, et al., Nat. Commun. 13 (2022) 2009.
[22] T. Zhang, F. Huo, C. Yin, Sens. Actuators B: Chem. 404 (2024) 135236.
[23] Y. Xu, C. Li, X. Ma, et al., Proc. Natl. Acad. Sci. U. S. A. 119 (2022) e2209904119.
[24] C. Ding, T. Ren, Coord. Chem. Rev. 482 (2023) 215080.
[25] Y. Xu, C. Li, J. An, et al., Sci. China Chem. 66 (2023) 155–163.
[26] X. Xing, E. Pang, S. Zhao, et al., Chin. Chem. Lett. 35 (2024) 108467.
[27] W. Li, R. Li, R. Chen, et al., Anal. Chem. 93 (2021) 8978–8985.
[28] O. Liba, A. de la Zerda, Nat. Biomed. Eng. 1 (2017) 0075.
[29] A.B.E. Attia, G. Balasundaram, M. Moothanchery, et al., Photoacoustics 16 (2019) 100144.
[30] I. Steinberg, D.M. Huland, O. Vermesh, et al., Photoacoustics 14 (2019) 77–98.
[31] D. Sun, Z. Chen, J. Hu, et al., Chin. Chem. Lett. 33 (2022) 4478–4494.
[32] G. Yin, T. Niu, Y. Gan, et al., Angew. Chem. Int. Ed. 57 (2018) 4991–4994.
[33] Y. Wen, W. Zhang, T. Liu, et al., Anal. Chem. 89 (2017) 11869–11874.
[34] J. Guo, B. Fang, H. Bai, et al., Trends Anal. Chem. 155 (2022) 116697.
[35] G.I. Giles, K.M. Tasker, C. Jacob, Free Radic, Biol. Med. 31 (2001) 1279–1283.
[36] G.I. Giles, K.M. Tasker, C. Collins, et al., Biochem. J. 364 (2002) 579–585.
[37] M.E. Suliman, P. Stenvinkel, O. Heimbürger, et al., Am. J. Kidney Dis. 40 (2002) 480–488.
[38] T. Rehman, M.A. Shabbir, M. Inam-Ur-Raheem, et al., Food Sci. Nutr. 8 (2020) 4696–4707.
[39] A. Pastore, A. Alisi, G. Di Giovamberardino, et al., Int. J. Mol. Sci. 15 (2014) 21202–21214.
[40] W. Zhao, H. Cheng, Y. Zhu, J. Clin. Lab. Anal. 34 (2020) e23202.
[41] N. Krahmer, R.V. Farese, T.C. Walther, EMBO Mol. Med. 5 (2013) 973–983.
[42] H. Wang, H. Zheng, W. Zhang, et al., Sens. Actuators B: Chem. 394 (2023) 134347.
[43] H. Song, W. Zhang, Y. Zhang, et al., Chem. Eng. J. 445 (2022) 136448.
[44] A.Kumar Ravi, S. Bhattacharyya, et al., EMBO J. 42 (2023) e114093.